Scattering phase delay and momentum transfer of light in disordered media

Pavel Yazhgur, Geoffroy Aubry, Luis Froufe-Pérez, Frank Scheffold

Scattering phase delay and momentum transfer of light in disordered media

Pavel Yazhgur,[1,*] Geoffroy J. Aubry,[1,2] Luis S. Froufe-Pérez,[1] and Frank Scheffold[1,†]
[1]*Department of Physics, University of Fribourg, CH-1700 Fribourg, Switzerland*
[2]*Université Côte d'Azur, CNRS, Institut de Physique de Nice, 06100 Nice, France*

(Received 6 October 2021; accepted 26 May 2022; published 22 June 2022)

Disordered dielectric materials with short-range spatial correlations on length scales comparable to the wavelength of light display a rich variety of optical phenomena: photonic band gaps, structural coloring, strong scattering, and whiteness. However, a lack of reliable and straightforward analytical models complicates the rationale design of optical materials for specific applications. Here, we demonstrate how to accurately introduce collective scattering and define the effective medium in single scattering from heterogeneous dielectrics with a substantial refractive index contrast, starting from fundamental principles. Our model captures the effective medium's role in the momentum transfer definition for the particle form and structure factor in the forward scattering regime. We support our claims through transfer matrix calculations scattering from particle clusters.

DOI: 10.1103/PhysRevResearch.4.023235

I. INTRODUCTION

Research on nanostructured and correlated dielectric materials is flourishing and generates a demand for efficient modeling of their optical properties. Applications for these materials are found as filters and switches, structural coloring in packing, solar cells, cosmetics and sensing, optical forces, whiteness for optical diffusers and screens, as well as increased transparency in multicomponent composite materials [1–18]. Selective forward scattering dielectric metamaterials and surfaces provide high transmission and subwavelength spatial wave control [19,20]. For ordered crystalline structures, the periodicity allows for an efficient and fast numerical computation of the optical properties even for a high index contrast [21]. The disordered nature of amorphous photonic materials, however, strongly limits the system size that can be handled within a reasonable computation time using conventional numerical techniques [1].

Analytical models that describe scattering from disordered dielectric materials, such as dense suspensions, colloidal clusters, or dielectric networks usually start from the weak scattering limit, also known as Rayleigh-Gans-Debye (RGD) theory. Unfortunately, the RGD approximation has a very limited range of validity: It requires both low refractive index contrast $|m-1| \ll 1$ and characteristic particle size $|m-1|kR \ll 1$ [22], where $k = 2\pi/\lambda$ denotes the wavenumber, R the particle radius, and $m = n_\mathrm{p}/n_\mathrm{h}$ is the ratio of the refractive indices of the scatter n_p and the host medium n_h. Most strikingly, the RGD theory cannot make any predictions about the effective medium correction that is required to account for deviations between spectral model predictions and experimental or numerical data [15,23–25]. Common electromagnetic mixing formulas, such as Bruggeman or Maxwell-Garnett, homogenize a medium in the limit $kR \ll 1$. Still, they are *a priori* not applicable to scattering from systems composed of building blocks with sizes comparable to the wavelength [26–29]. Due to these limitations of the RGD theory and the lack of alternative approaches, the role of the effective medium on scattering and propagation of light in "optically soft" disordered dielectrics—meaning materials with a moderate index contrast—is essentially unresolved. In multiple light scattering and photon diffusion, successive single scattering events occur over distances of the scattering mean free path ℓ_s. A better understanding of the single scattering function is thus vital for the description of light propagation in such dense media. However, the existing knowledge gap makes it possible that contradictory results remain unchallenged and cannot be resolved. For example, in a recent article, Rezvani Naraghi *et al.* [30] claim that near-field coupling, a phenomenon expected for high index and resonant scatterers [31,32], enhances the optical transmission already for dense aqueous silica particle suspensions with $R \sim \lambda$ and $|m-1| = 0.13$, although previous work on polystyrene scatterers ($|m-1| = 0.2$) of similar size has shown no such effect [33].

A substantial refractive index contrast can influence the scattering process in dense dielectrics locally and globally. Locally, near-field coupling between building blocks may play an important role [34], as well as Mie resonances [22] and internal reflections, leading to phenomena like whispering gallery modes [35]. Globally, a finite index contrast $|m-1|$ increases the optical path length or, equivalently, creates a delay of the wave's phase. Consequently, the momentum transfer $\boldsymbol{q}$, defined in the RGD theory, as the vectorial difference between the incoming $\boldsymbol{k}_\mathrm{in}$ and the scattered wave vector

*pavel.yazhgur@unifr.ch
†frank.scheffold@unifr.ch

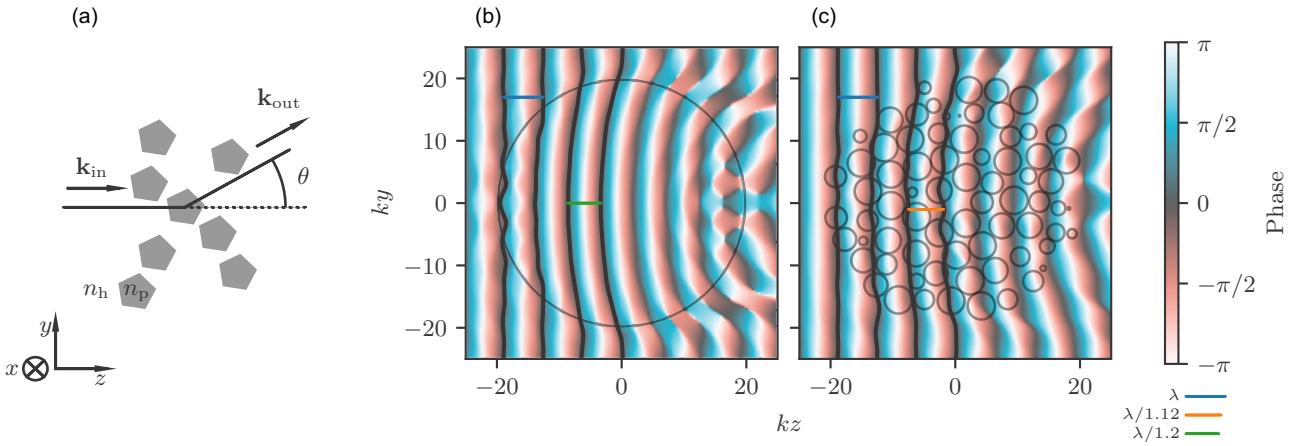

FIG. 1. Phase maps in light scattering from soft dielectrics. (a) Scattering geometry with an incoming plane wave $\boldsymbol{k}_{\rm in}$ propagating in z direction and a scattered wave $\boldsymbol{k}_{\rm out}$. (b) Phase map calculated using Mie theory (equatorial cross section, incoming field perpendicular to the plane) inside a sphere illuminated with a plane wave, $kR = 19.8$, $m = 1.2$. (c) Phase map calculated using the T-matrix approach inside a spherical cluster containing $N = 435$ dielectric spheres illuminated with a plane wave, $kR = 2.2$, $m = 1.2$. The coloured bars show the distance (wavelength) between the wave fronts having the same phase ($\phi = 0$) in different materials.

$\boldsymbol{k}_{\rm out}$, is influenced by the effective medium. Previous studies of scattering from dense particle assemblies define an effective scattering momentum transfer $\boldsymbol{q}_{\rm eff} \equiv \boldsymbol{q}_0 n_{\rm eff}$, where $\boldsymbol{q}_0$ is the vacuum's momentum transfer and $n_{\rm eff}$ is an effective refractive index. $n_{\rm eff}$ has been obtained by either using the homogenized effective index [24,36], the host-medium index [33], or something in between [37]; for example, using the coherent potential approximation (CPA) [23,38,39]. The choice of the effective index, however, is often uncontrolled and merely provides an additional parameter to fit the experimental or numerical data [37]. In the present paper, we systematically derive a correction to RGD for heterogeneous, optically soft dielectrics, leading to a rigorous definition of the effective momentum transfer $\boldsymbol{q}_{\rm eff}$. To this end, we show how to introduce the effective medium in a controlled way via the phase delay [40,41].

II. ELECTROMAGNETIC THEORY

We base our discussion on the integral formulation of the scattering problem, which can be expressed in an exact form for any dielectric scattering material embedded in a host medium [16,22]. Consider a material with relative permittivity $\varepsilon(\boldsymbol{r}')$ in a host medium with relative permittivity $\varepsilon_{\rm h}$. In the far field the electric field of the scattered wave $\boldsymbol{E}_{\rm s}(\boldsymbol{r})$ can be linked to the susceptibility, $\chi(\boldsymbol{r}') = \varepsilon(\boldsymbol{r}')/\varepsilon_{\rm h} - 1$, and to the electric field due to the incoming wave inside the scattering medium $\boldsymbol{E}(\boldsymbol{r}')$ as (see Appendix A for details)

$$\boldsymbol{E}_{\rm s}(\boldsymbol{r}) = \frac{e^{ikr}}{r}\frac{k^2}{4\pi\varepsilon_0\varepsilon_{\rm h}}(\mathbb{I} - \hat{\boldsymbol{u}}_{\rm out}\otimes\hat{\boldsymbol{u}}_{\rm out})\boldsymbol{p}(\hat{\boldsymbol{u}}_{\rm out}), \tag{1}$$

where the total dipole $\boldsymbol{p}(\hat{\boldsymbol{u}}_{\rm out})$ (direction dependent) is

$$\boldsymbol{p}(\hat{\boldsymbol{u}}_{\rm out}) \equiv \varepsilon_0\varepsilon_{\rm h}\int d^3\boldsymbol{r}' e^{-i\boldsymbol{k}_{\rm out}\cdot\boldsymbol{r}'}\chi(\boldsymbol{r}')\boldsymbol{E}(\boldsymbol{r}'), \tag{2}$$

$k = 2\pi n_{\rm h}/\lambda_0$ is the wavenumber, λ_0 denotes the wavelength in vacuum, and $\boldsymbol{k}_{\rm out} = k\hat{\boldsymbol{u}}_{\rm out}$ is the wave vector of scattered light. The integral defining $\boldsymbol{p}(\hat{\boldsymbol{u}}_{\rm out})$ is taken over the scattering volume. We consider an incident plane wave $\boldsymbol{E}_{\rm in}(\boldsymbol{r}) = E_0\hat{\boldsymbol{u}}_{\rm pol}e^{i\boldsymbol{k}_{\rm in}\cdot\boldsymbol{r}}$ polarized along the direction $\hat{\boldsymbol{u}}_{\rm pol}$, whose intensity is $I_{\rm in} = |E_0|^2/(2Z)$, $Z \equiv \sqrt{\mu_0/\varepsilon_0}\sqrt{1/\varepsilon_{\rm h}}$ being the host medium impedance. The differential scattering cross section (SCS) in the direction $\hat{\boldsymbol{u}}_{\rm out}$ reads

$$\frac{d\sigma_s(\hat{\boldsymbol{u}}_{\rm out})}{d\Omega} = \frac{1}{k^2}(|\boldsymbol{f}(\hat{\boldsymbol{u}}_{\rm out})|^2 - |\hat{\boldsymbol{u}}_{\rm out}\cdot\boldsymbol{f}(\hat{\boldsymbol{u}}_{\rm out})|^2), \tag{3}$$

where we introduce the dimensionless field $\boldsymbol{f}(\hat{\boldsymbol{u}}_{\rm out}) \equiv \frac{k^3}{4\pi\varepsilon_0\varepsilon_h}\boldsymbol{p}(\hat{\boldsymbol{u}}_{\rm out})/E_0$. For simplicity, in the following, we only consider scattering in the yz-plane with an incident wave's electric field polarized perpendicularly to this plane, and thus we can assume $\boldsymbol{k}_{\rm in} = k\hat{\boldsymbol{u}}_z$ and $\hat{\boldsymbol{u}}_{\rm pol} = \hat{\boldsymbol{u}}_x$ [see Fig. 1(a) for the scattering geometry]. Furthermore, we assume that the local electric field is collinear to the incoming field, $\boldsymbol{f}(\hat{\boldsymbol{u}}_{\rm out}) = f(\theta)\hat{\boldsymbol{u}}_x$, i.e., the scattered field is perpendicular to the scattering plane and only depends on the θ angle (see also Appendix B).

A. Modified momentum transfer

Equation (3) is exact but can only be solved for a spherical scatterer using Mie's theory [42] or the Debye series [43]. In general, the far-field scattered wave depends on the local field inside the scatterer, $\boldsymbol{E}(\boldsymbol{r}')$ in Eq. (2), which is *a priori* unknown. However, Eq. (3) can be solved by approximating the local field. In the simplest case one replaces the local field by the unperturbed incident field, which corresponds to the RGD limit. Based on this assumption, it is straightforward to calculate a sphere's differential SCS angular dependence $\frac{d\sigma(\theta)}{d\Omega} = \frac{|f(\theta)|^2}{k^2}$ —proportional to the particle form factor $F(\boldsymbol{q}) \equiv V^{-1}\int_V d^3\boldsymbol{r}e^{-i\boldsymbol{q}\cdot\boldsymbol{r}}$—as shown, e.g., in Refs. [42,44], $f(q) = \frac{k^3V}{4\pi}\chi F(q) = \frac{k^3V}{4\pi}\chi\frac{3j_1(qR)}{qR}$, where $j_1(x) = (\sin x - x\cos x)/x^2$ is the first-order spherical Bessel function of the first kind and $\chi = \epsilon_p/\epsilon_h - 1$. In the RGD-theory, the scattering momentum transfer is given by the norm of the scattering vector $q = |\boldsymbol{q}| = |\boldsymbol{k}_{\rm out} - \boldsymbol{k}_{\rm in}| = 2k\sin(\theta/2)$. For a sphere of radius R, the form factor $F(q) = 3j_1(qR)/qR$ only depends on the modulus of $\boldsymbol{q}$.

For a more accurate theoretical description going beyond RGD, Saxon proposed already in 1955 to replace the incident field's phase by the phase inside the particle $m \cdot \boldsymbol{k}_{\text{in}} \cdot \boldsymbol{r}'$: $\boldsymbol{E}(\boldsymbol{r}') = E_0 \hat{\boldsymbol{u}}_{\text{pol}} e^{im\boldsymbol{k}_{\text{in}} \cdot \boldsymbol{r}'}$ [45]. This idea was later taken up by Shimizu [46] and Gordon [47] in the 1980s but never became widely used. Further assumptions about the field inside the dielectric medium can be added to the model, as discussed by Gordon [47], but are not considered in the present paper. Using the local field approximation by Saxon and Gordon [45,47], we obtain a modified momentum transfer $\boldsymbol{q}_{\text{mod}}$

$$\boldsymbol{q}_{\text{mod}} = \boldsymbol{k}_{\text{out}} - m \cdot \boldsymbol{k}_{\text{in}}, \tag{4}$$

$$q_{\text{mod}}^2 = k^2(m^2 + 1 - 2m\cos\theta), \tag{5}$$

which, for $m \to 1$, using $1 - \cos(\theta) = 2(\sin(\theta/2))^2$, approaches the usual RGD-result. Although Eq. (4) and Eq. (5) are known in the literature, the consequences of this model have not been fully explored nor applied to complex, mixed dielectrics. Compared to RGD, the modified RGD (mRGD) yields much better agreement with Mie scattering by spheres, especially in the forward scattering direction and concerning the position of the minima as shown in Fig. 2(a). Plotted as a function of $q_{\text{mod}}R$, the scattering data nearly collapse on a master curve, Fig. 2(b). We remark that for sufficiently small $q_{\text{mod}}R$, below the first minima, the mRGD approximation perfectly agrees with the Mie scattering result. Even for large kR and moderate to large values of m, the mRGD approximation still provides a good overall agreement with the Mie theory in a regime where the classical RGD model fails. We also notice from Eq. (5) that for $m > 1$, the effective momentum transfer q_{mod} remains nonzero even for $\theta \to 0$ with $q_{\text{mod}}(0)R = kR\sqrt{m^2 - 2m + 1} = kR|m - 1|$. As we increase m, the minima of the scattering function are pushed to smaller angles and eventually disappear at discrete values of m. For example, the first zero of $j_1(x)^2$ is located at $x = q_{\text{mod}}(\theta)R = 4.493$ and therefore for $q_{\text{mod}}(0)R > 4.493$ it cannot be reached anymore, Fig. 3.

B. Wentzel-Kramers-Brillouin approximation (WKBA)

The influence of the particle curvature on the phase delay and momentum transfer can be taken into account using the Wentzel-Kramers-Brillouin approximation (WKBA) [40] that calculates the phase delay that each ray experiences inside the medium prior to scattering. If we assume that the incoming plane wave propagates rectilinear in the positive z direction, the phase at each point can be written as $\phi(\boldsymbol{r}') = kz' + k\int_{-\infty}^{z'}[m(z) - 1]dz$, where we integrate along the rectilinear path with $x, y = \text{const}$. The corresponding electric field $\boldsymbol{E}(\boldsymbol{r}') = E_0 \hat{\boldsymbol{u}}_{\text{pol}} e^{i\phi(\boldsymbol{r}')}$ then can be plugged into Eq. (2). For spherical particles Eq. (2) reduces to a 1D integral [48]. The WKBA-differential SCS of a sphere is plotted in Fig. 2(a) for $m = 1.2$ and $kR = 6.5$. One can remark that WKBA predicts a scattering curve almost identical to the mRGD model. The main significant improvement of WKBA compared to mRGD is the removal of the scattering singularities, or zero intensities, at the minima position. The WKBA and mRGD accurately predict forward scattering, as shown in the inset of Fig. 2(b), which holds even up to large m values (WKBA-prediction is identical for $\theta = 0$). The WKBA- and mRGD-predictions lose accuracy at backscattering angles $\theta > 90°$.

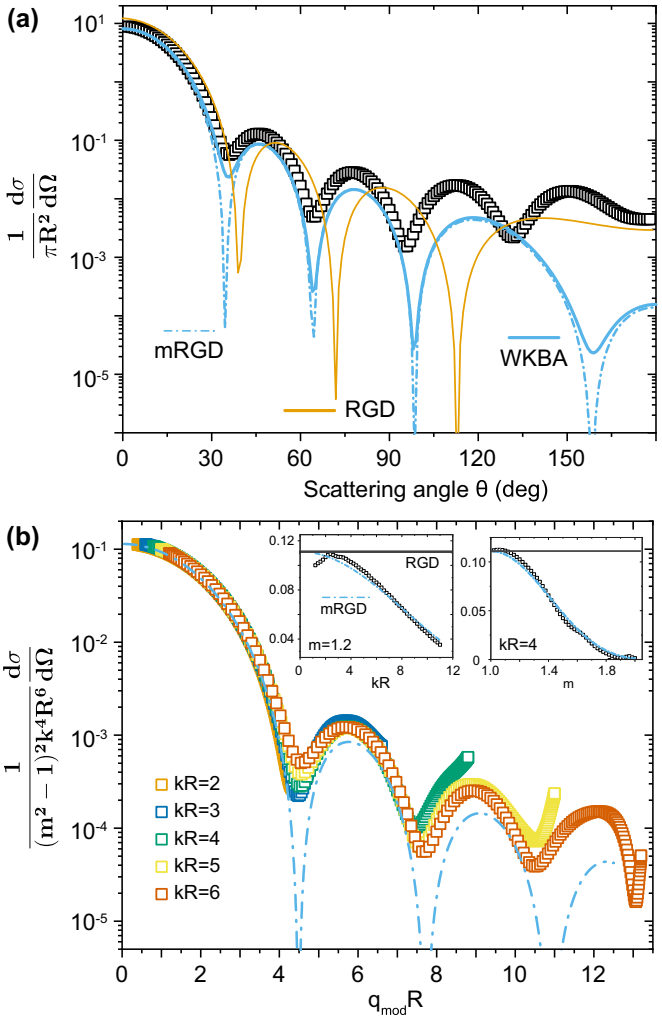

FIG. 2. (a) Angular dependence of the differential scattering cross-section (SCS) of single dielectric spheres with $m = 1.2$, $kR = 6.5$. Open symbols show the prediction by Mie theory and the lines are predicted by single scattering approximations RGD (orange line), mRGD (dash-dotted blue line), and WKBA (solid-blue line). (b) Mie differential scattering cross-section (SCS) for $m = 1.2$ and $kR \in [2, 6]$ plotted as a function of $q_{\text{mod}}R$, see Eq. (5). Dash-dotted blue line: mRGD approximation. Inset: Mie differential scattering cross section at $\theta = 0$ (open symbols) for different particle sizes (left) and refractive indices (right). Dash-dotted lines show the mRGD-prediction (WKBA-prediction for $\theta = 0$ is identical). The horizontal lines show the RGD prediction.

Next, we address scattering from mixed dielectrics. To develop the main concepts, we restrict the quantitative discussion to the case of a dense assembly of N dielectric spheres densely packed in a large metaball. We first derive an approximate expression for $\boldsymbol{E}(\boldsymbol{r}')$, and then calculate the far-field scattered intensity and the differential SCS. Numerically we generate dense packings of identical polystyrene particles suspended in water (filling fraction $\phi = 0.6$, $m = 1.2$) by running a force-biased generation algorithm followed by a molecular dynamics equilibration using the PackingGeneration project [49]. Figure 1(b), shows the Mie analysis of

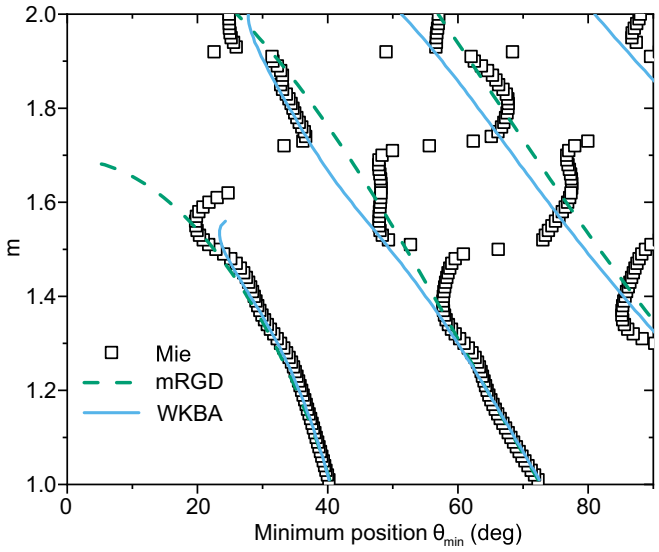

FIG. 3. Shift of the position of the minima of the scattering function $\theta_{\min}$ with increasing m. Open squares: predictions by Mie theory for a dielectric sphere with $kR = 6.5$. The plot shows sharp transitions, e.g., around $m = 1.6$ where the first minimum disappears. Dashed lines: prediction for the minima position from mRGD for $kR = 6.5$, solving $q_{\text{mod}}R = x_{\min}$ for values where $j(x_{\min}) = 0$. Solid lines: prediction from WKBA model.

the field inside a dielectric sphere $m = 1.2$ [22]. The results support Saxon's proposal; the wavefronts remain relatively flat, but the wavelength of the incident wave is reduced by a factor m. We use the multiple sphere T-matrix method (MSTM open-source code [50]) to numerically calculate the field propagating inside the densely packed assemblies of particles, Fig. 1(c). The wavefronts still overall resemble a plane wave but with a wavelength rescaled by an effective refractive index ratio m_{eff}. From the calculations of the spatial field distribution for $N = 435$, $m = 1.2$, we extract $m_{\text{eff}} \approx 1.12$, a value that is very close to Maxwell-Garnett (MG) effective medium prediction m_{MG}.

WKBA assumes that the local fields exciting each scatterer in the ensemble correspond to plane waves with a phase given by the optical path length traversed by the input field in the effective medium. In a purely numerical implementation using ray tracing, the WKB-approximation can be applied to any mixed dielectric such as sphere assemblies, see Fig. 4(a), but also to bicontinuous materials such as dielectric hyperuniform, diamond, or foam-like networks [51–54].

III. SCATTERING FROM PARTICLE CLUSTERS

We consider the case of sphere-packings in a finite-sized spherical cluster, Figs. 1(b) and 1(c), for which we can derive a closed-form analytical result. For a scattering element $\boldsymbol{r}'$ inside a given sphere, index i, the integral can be split into $\phi(\boldsymbol{r}') = kz' + k\int_{z_0}^{z_i}(m(z)-1)dz + k\int_{z_i}^{z'}(m-1)dz$. The first integral describes the phase delay acquired on the path starting at z_0 to z_i, sitting on a plane normal to $\boldsymbol{u}_z$ through the ith-particle's center. In a mean-field approach, we approximate $m(z) \simeq m_{\text{eff}}$ where $m_{\text{eff}} = (\phi n_p + (1-\phi)n_h)/n_h$ is the weighted average of the refractive index ratio of the two material components (for $|m-1| < 0.5$, $m_{\text{eff}} \simeq m_{\text{MG}}$ [27]). Thus $\int_{z_0}^{z_i}(m(z)-1)dz \simeq (m_{\text{eff}}-1)(z_i - z_0)$. The second integral is taken fully inside the dielectric material, so we can evaluate it immediately. We find $\phi(z') = km(z'-z_i) + km_{\text{eff}}z_i - k(m_{\text{eff}}-1)z_0$. The last term can be dropped if we assume all rays start on the same plane $z_0 = \text{constant}$, thus neglecting the spherical cluster's shape curvature [55]. Since $\boldsymbol{k}_{\text{in}} = k\boldsymbol{u}_z$, we can return to the vector notation and write

$$\boldsymbol{E}(\boldsymbol{r}') = \sum_i [\boldsymbol{r}' \in i]\boldsymbol{E_0} e^{im\boldsymbol{k}_{\text{in}}\cdot(\boldsymbol{r}'-\boldsymbol{r}_i)+im_{\text{eff}}\boldsymbol{k}_{\text{in}}\cdot\boldsymbol{r}_i}, \tag{6}$$

where $[\boldsymbol{r}' \in i]$ is the indicator function of the particle i. When applied to a periodic structure, such as an opal photonic crystal, the expression for the inner electric field respects Bloch's theorem, which demonstrates the consistency of our approach. The latter becomes apparent if we rewrite Eq. (6) as follows:

$$\boldsymbol{E}(\boldsymbol{r}') = \boldsymbol{E_0} e^{im_{\text{eff}}\boldsymbol{k}_{\text{in}}\cdot\boldsymbol{r}'} \sum_i [\boldsymbol{r}' \in i] e^{i(m-m_{\text{eff}})\boldsymbol{k}_{\text{in}}\cdot(\boldsymbol{r}'-\boldsymbol{r}_i)}, \tag{7}$$

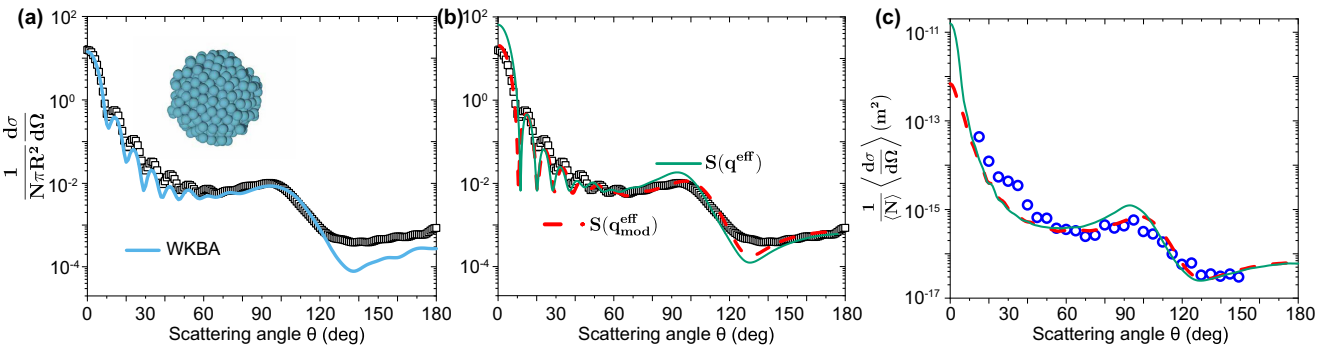

FIG. 4. Scattering from a cluster of $N = 435$ particles with $kR = 2.2$ and $m = 1.2$, panel (a) and (b). Open squares: T-matrix calculations of a cluster shown in the inset of panel (a). The solid line in panel (a) shows the numerical WKBA (ray tracing) prediction. (b) Lines: predictions by the closed-form analytical model Eq. (10) using either q^{eff} or $q^{\text{eff}}_{\text{mod}}$ for the structure factor. (c) Experimental differential scattering cross section of dilute dispersions of spherical particle clusters (mean diameter $\overline{d}_{\text{PB}} = 3.3\ \mu$m, polydispersity $\delta d_{\text{PB}}/\overline{d}_{\text{PB}} \sim 0.45$) suspended in water ($n_{\text{h}} = 1.33$) measured by static light scattering, $\lambda = 660$ nm [36]. The clusters are made of closely packed $R = 174$ nm ($kR \approx 2.2$) polystyrene spheres ($n_{\text{p}} = 1.59$) with a polydispersity of ∼5% and a filling fraction of $\phi \sim 0.6$ [36]. Lines: same color label as in panel (b), calculated using Eq. (9) with Mie scattering amplitudes and averaged over the PB-size distribution.

which shows that $\boldsymbol{E}(\boldsymbol{r}')$ is a product of a plane wave and a periodic function.

With Eq. (2) and our definition of the modified momentum transfer in the effective medium $\boldsymbol{q}_{\rm mod}^{\rm eff} = \boldsymbol{k}_{\rm out} - m_{\rm eff}\boldsymbol{k}_{\rm in}$, we obtain the total dipole

$$\frac{\boldsymbol{p}(\hat{\boldsymbol{u}}_{\rm out})}{\varepsilon_0\varepsilon_h E_0} = \hat{\boldsymbol{u}}_{\rm pol}\sum_i e^{i\boldsymbol{q}_{\rm mod}^{\rm eff}\cdot\boldsymbol{r}_i}\int_{Vi}\chi e^{-i\boldsymbol{q}_{\rm mod}\cdot(\boldsymbol{r}'-\boldsymbol{r}_i)}d^3\boldsymbol{r}', \tag{8}$$

where each integration is performed over the volume of ith particle. The integral only depends on the shape of the particle, and thus the sum over particle positions i and the particle form factor factorize in the common way [44,56],

$$\boldsymbol{p}(\hat{\boldsymbol{u}}_{\rm out}) = \varepsilon_0\varepsilon_h E_0\hat{\boldsymbol{u}}_{\rm pol}\chi\sum V_i e^{i\boldsymbol{q}_{\rm mod}^{\rm eff}\cdot\boldsymbol{r}_i}F(q_{\rm mod}, R_i), \tag{9}$$

where R_i is the radius of the corresponding sphere. For monodisperse assemblies $R_i = R =$ constant, $F(q_{\rm mod}, R_i)$ can be taken out of the sum. Considering averages over all possible orientations we can drop the vector notation for the momentum transfer. Then the differential SCS for assemblies of identical particles with radius R is given by

$$\frac{d\sigma(\theta)}{d\Omega} = NS\big(q_{\rm mod}^{\rm eff}\big)\frac{d\sigma(\theta)}{d\Omega}_{\rm p}, \tag{10}$$

with $S(|\boldsymbol{x}|) = \frac{1}{N}\langle\sum_{p,p'}e^{i\boldsymbol{x}\cdot(\boldsymbol{r}_p-\boldsymbol{r}_{p'})}\rangle$ defined as a finite sum over particle $(p,\ p')$ centers inside the cluster, where the averaging is performed over various cluster configurations. Expression (10) strongly resembles the classical RGD-approximation ($|m-1|\to 0$), but now can be applied for a finite refractive index contrast $|m-1| < 0.2-0.5$. In a single scattering approximation for a mixed dielectric, the momentum transfer for collective scattering is set by the product of the structure factor, with a momentum transfer $q_{\rm mod}^{\rm eff}$, and the sphere differential SCS. For the latter we can use the mRGD or WBK approximation (with $q_{\rm mod}$), but we can also derive Eq. (10) retaining the full Mie solution for $(d\sigma(\theta)/d\Omega)_{\rm p}$ (Appendix A). In Fig. 4, we test the accuracy of the model predictions by comparison with exact MSTM numerical [50] and experimental results obtained for spherical random close-packed clusters.

Equation (10) using the Mie sphere differential SCS gives an accurate prediction for low-angle scattering [57]. At the same time, the commonly employed expression $\boldsymbol{q}^{\rm eff} = m_{\rm eff}(\boldsymbol{k}_{\rm out} - \boldsymbol{k}_{\rm in})$ catastrophically fails in the forward direction. In the back-scattering direction, however, scattering is weak; both definitions of $\boldsymbol{q}^{\rm eff}$ show deviations, and the level of agreement is comparable. In this regime, multiple scattering or internal reflections, not considered in the model, become increasingly important as $|m-1|$ increases.

IV. CONCLUSIONS

To conclude, we have shown how to accurately treat the phase delay and momentum transfer in single light scattering from optically soft, disordered dielectrics. The derivation and validation of Eqs. (9) and (10) using the WKB-approximation for assemblies of dielectric spheres is the central result of this paper. Furthermore, we explore the use of the WKBA and modified RGD concepts and suggest pathways to develop more accurate theoretical ways to describe scattering in heterogeneous dielectrics. Notably, we clarify the effective medium's role in the momentum transfer definition for the particle form and structure factor. Moreover, in a purely numerical implementation, the same approach, using ray tracing, can be applied to any structures, sphere assemblies, and bicontinuous materials such as dielectric hyperuniform, diamond, or foam-like networks, emphasizing the importance of our results. Finally, one can also use the single-scattering concepts derived in our paper as a basis to improve the modeling of diffuse transport in dense dielectrics.

The data shown in the figures and some of the underlying raw data are available on the online repository Zenodo [58].

ACKNOWLEDGMENTS

We thank Dave Pine for illuminating discussions and Tom Mason for help in accessing Saxons lecture notes, ref. [45], in the UCLA library. The Swiss National Science Foundation financially supported this work through the National Center of Competence in Research Bio-Inspired Materials Grant No. 182881, and Projects No. 188494, No. 183651, and No. 197146. The computations were performed using the OPAL infrastructure and the Center for High-Performance Computing from the Université Côte d'Azur (ANR-15-IDEX-01, Idex UCAJEDI).

APPENDIX A: GENERAL DERIVATION OF THE DIFFERENTIAL SCATTERING CROSS SECTION

The electromagnetic wave equation in the absence of sources (pure scattering) for a monochromatic field reads

$$\nabla\times\nabla\times\boldsymbol{E}(\boldsymbol{r}) - \left(\frac{\omega}{c}\right)^2\varepsilon(\boldsymbol{r})\boldsymbol{E}(\boldsymbol{r}) = 0, \tag{A1}$$

where we assume a piecewise constant relative permittivity function $\varepsilon(\boldsymbol{r})$ (in general complex and depending on the frequency ω). For a given incoming field $\boldsymbol{E}_{\rm in}(\boldsymbol{r})$, it satisfies the wave equation in a host medium with constant permittivity $\varepsilon(\boldsymbol{r}) \equiv \varepsilon_{\rm h}$, and we can recast equation (A1) to

$$\nabla\times\nabla\times\boldsymbol{E}(\boldsymbol{r}) - \left(\frac{\omega}{c}\right)^2\varepsilon_{\rm h}\boldsymbol{E}(\boldsymbol{r}) = \left(\frac{\omega}{c}\right)^2\varepsilon_0\varepsilon_{\rm h}\chi(\boldsymbol{r})\boldsymbol{E}(\boldsymbol{r}), \tag{A2}$$

where the susceptibility relative to the host medium is defined as $\chi(\boldsymbol{r}) \equiv (\varepsilon(\boldsymbol{r}) - \varepsilon_{\rm h})/\varepsilon_{\rm h}$. That takes the form of the wave equation in the host medium with additional sources given by a polarization current density $\boldsymbol{P}(\boldsymbol{r}) \equiv \varepsilon_0\varepsilon_{\rm h}\chi\boldsymbol{E}(\boldsymbol{r})$. The scattered field is given by the particular solution to equation (A2) with radiation boundary conditions. Considering the Green tensor for the electromagnetic field $\mathbb{G}(\boldsymbol{r},\boldsymbol{r}')$, the total scattered electric $\boldsymbol{E}_{\rm s}(\boldsymbol{r})$ field is given by

$$\boldsymbol{E}_{\rm s}(\boldsymbol{r}) = \frac{k^2}{\varepsilon_0\varepsilon_h}\int d^3\boldsymbol{r}'\mathbb{G}_E(\boldsymbol{r},\boldsymbol{r}')\boldsymbol{P}(\boldsymbol{r}'), \tag{A3}$$

where $k = 2\pi n_{\rm h}/\lambda_0$ is the host wave number of the input wave. Taking the far-field approximation of the Green tensor,

$$\mathbb{G}_E(\boldsymbol{r},\boldsymbol{r}') \simeq \frac{e^{ikr}}{4\pi r}(\mathbb{I} - \hat{\boldsymbol{u}}_{\rm out}\otimes\hat{\boldsymbol{u}}_{\rm out})e^{-i\boldsymbol{k}_{\rm out}\cdot\boldsymbol{r}'}, \tag{A4}$$

where $\boldsymbol{k}_{\rm out} = k\hat{\boldsymbol{u}}_{\rm out}$, and $\hat{\boldsymbol{u}}_{\rm out} = \boldsymbol{r}/|\boldsymbol{r}|$, we obtain

$$\boldsymbol{E}_{\rm s}(\boldsymbol{r}) = \frac{e^{ikr}}{r}\frac{k^2}{4\pi\varepsilon_0\varepsilon_{\rm h}}(\mathbb{I} - \hat{\boldsymbol{u}}_{\rm out}\otimes\hat{\boldsymbol{u}}_{\rm out})\boldsymbol{p}(\hat{\boldsymbol{u}}_{\rm out}), \tag{A5}$$

where the total dipole $\hat{\boldsymbol{p}}_{\rm out}$ (depending on the direction $\hat{\boldsymbol{u}}_{\rm out}$) is defined as

$$\hat{\boldsymbol{p}}_{\rm out} \equiv \int d^3\boldsymbol{r}' e^{-i\boldsymbol{k}_{\rm out}\cdot\boldsymbol{r}'}\boldsymbol{P}(\boldsymbol{r}'). \tag{A6}$$

Equation (A6) holds for any scalar permittivity and assumes a magnetic permeability equal to the vacuum one. Taking the curl of the scattered electric field, we obtain the scattered magnetic field in the far-field approximation

$$\boldsymbol{H}_{\rm s}(\boldsymbol{r}) = \frac{e^{ikr}}{r}\frac{k^2}{4\pi\varepsilon_0\varepsilon_{\rm h}Z}\hat{\boldsymbol{u}}_{\rm out}\times\boldsymbol{p}(\hat{\boldsymbol{u}}_{\rm out}), \tag{A7}$$

where Z stands for the host medium impedance $Z \equiv \sqrt{\frac{\mu_0}{\varepsilon_0}}\sqrt{1/\varepsilon_{\rm h}}$. The scattering Poynting vector $\boldsymbol{S}(\boldsymbol{r}) = 1/2\Re(\boldsymbol{E}_{\rm s}(\boldsymbol{r})\times\boldsymbol{H}_{\rm s}^*(\boldsymbol{r}))$ is given by

$$\boldsymbol{S}(\boldsymbol{r}) = \frac{\hat{\boldsymbol{u}}_{\rm out}}{2Z}\left(\frac{k^4}{4\pi\varepsilon_0\varepsilon_{\rm h}}\right)^2(|\boldsymbol{p}(\hat{\boldsymbol{u}}_{\rm out})|^2 - |\hat{\boldsymbol{u}}_{\rm out}\cdot\boldsymbol{p}(\hat{\boldsymbol{u}}_{\rm out})|^2). \tag{A8}$$

The incoming field $\boldsymbol{E}_{\rm in}(\boldsymbol{r})$ is a plane wave

$$\boldsymbol{E}_{\rm in}(\boldsymbol{r}) = E_0\hat{\boldsymbol{u}}_{\rm pol}e^{i\boldsymbol{k}_{\rm in}\cdot\boldsymbol{r}} \tag{A9}$$

of amplitude E_0 and polarization vector $\hat{\boldsymbol{u}}_{\rm pol}$, whose intensity is $I_0 = |E_0|^2/(2Z)$. The differential SCS is defined as the ratio of the scattered power per unit solid angle in a given direction to the input intensity

$$\frac{d\sigma_{\rm s}(\hat{\boldsymbol{u}}_{\rm out})}{d\Omega} = \frac{\boldsymbol{S}(\boldsymbol{r})\cdot\hat{\boldsymbol{u}}_{\rm out}}{I_{\rm in}}r^2 = \frac{1}{k^2}(|\boldsymbol{f}(\hat{\boldsymbol{u}}_{\rm out})|^2 - |\hat{\boldsymbol{u}}_{\rm out}\cdot\boldsymbol{f}(\hat{\boldsymbol{u}}_{\rm out})|^2), \tag{A10}$$

where $\boldsymbol{f}(\hat{\boldsymbol{u}}_{\rm out})$ is defined as in the main text,

$$\boldsymbol{f}(\hat{\boldsymbol{u}}_{\rm out}) \equiv \frac{k^3}{4\pi\varepsilon_0\varepsilon_{\rm h}}\boldsymbol{p}(\hat{\boldsymbol{u}}_{\rm out})/E_0. \tag{A11}$$

If the input field presents an additional phase delay, $\boldsymbol{E}_{\rm in}(\boldsymbol{r},\phi) = \boldsymbol{E}_{\rm in}(\boldsymbol{r},\phi)e^{i\phi}$, so will the polarization current density and the total dipole, i.e., $\boldsymbol{P}(\boldsymbol{r}',\phi) = \boldsymbol{P}(\boldsymbol{r}')e^{i\boldsymbol{\phi}}$, $\boldsymbol{p}(\hat{\boldsymbol{u}}_{\rm out},\phi) = \boldsymbol{p}(\hat{\boldsymbol{u}}_{\rm out})e^{i\phi}$, and analogous phase delays will also be present in the scattered fields. We make the assumption that the local fields exciting each individual scatter (i) in the ensemble is a plane wave with a phase given by the optical path length traversed by the input field in the effective medium,

$$\phi_i = kz_{0,i} + km_{\rm eff}(z_i - z_{0,i}), \tag{A12}$$

where $z_{0,i}$ is the input point of the plane wave impinging on the spherical particle cluster. If we neglect curvature effects, $z_{0,i} = z_0$ common to all scatters, we have

$$\phi_i = km_{\rm eff}z_i + k(1 - m_{\rm eff})z_0. \tag{A13}$$

The field scattered by each particle will carry an additional phase ϕ_i, depending on the scatter position, due to the effective medium. This approximation leads to the differential SCS

$$\frac{d\sigma_{\rm s}(\hat{\boldsymbol{u}}_{\rm out})}{d\Omega} = NS\big(q_{\rm mod}^{\rm eff}\big)\frac{d\sigma(\theta)}{d\Omega}_{\rm NP}. \tag{A14}$$

The total dipole $\hat{\boldsymbol{p}}_{\rm out}$, Eq. (A6), depends on the complete solution of the scattering problem, i.e., the total electric field inside the scattering medium $\boldsymbol{E}(\boldsymbol{r})$. In general, we divide the system into discrete elementary dipoles and apply approximations such as the mRGD or the numerical WKB (ray tracing). In the case of sphere assemblies, however, where the complete Mie scattering solution of a sphere is known, we can substitute the complete Mie scattering solution inside the sphere to get an exact value of the total dipole $\boldsymbol{p}(\hat{\boldsymbol{u}}_{\rm out})$.

APPENDIX B: ELECTRIC FIELD INSIDE DIELECTRIC PARTICLES

In the mRGD, and WKBA approximation, we only correct the phase of the field inside the scattering material. The field amplitude is kept unchanged. Even for a moderate index contrast, this assumption is not always well fulfilled. For small particles $k \ll R$ (in the Rayleigh limit) one should use the electrostatic result $E = \frac{3}{m^2+2}E_0$ [22]. The latter is also responsible for the drop of the zero angle Mie differential SCS for kR less than two observed in Fig. 2. However, for $|m-1|$, $|m-1| \lesssim 0.4$ and $kR \gtrsim 1$, the inner field amplitude is close to the incoming one, as assumed in our model [22].

APPENDIX C: PREPARATION OF COLLOIDAL PARTICLE CLUSTERS

As described earlier in Ref. [36] we synthesize polystyrene colloidal particles by standard surfactant-free polymerization using 4-vinylbenzene sulfonate as an ionic comonomer. From static light scattering (SLS), the average diameter of the spheres is 348 nm with a typical polydispersity of 5%. We prepare particle clusters using a solvent-drying method. For this purpose, we add about 20 μL of aqueous particle dispersion with a volume fraction of 1% to 1 mL of anhydrous decanol. We obtain a water/particle-in-oil emulsion using a vortex mixer at 2700 rpm for 20 seconds. Since water is sparingly soluble in decanol, the droplets shrink rapidly, leading to the formation of solid spherical clusters. We purify the clusters by centrifugation and redispersing them several times in isopropanol. In a final step, we replace the isopropanol by purified water. We add a 5 mM KCl electrolyte to stabilize the clusters against aggregation. We determine the mean size and cluster size distribution by image analysis based on scanning electron microscopy images (SEM).

APPENDIX D: STATIC LIGHT SCATTERING EXPERIMENTS

As described earlier in Ref. [36] we acquire experimental differential cross-sectional data by static light scattering (SLS) with a commercial scattered light spectrometer-goniometer (LS Instruments, Fribourg, Switzerland) operating at a laser wavelength of $\lambda = 660$ nm and covering scattering angles θ from 15° to 150°. For the calibration of the absolute scale data, we use toluene.

[1] K. Vynck, R. Pierrat, R. Carminati, L. S. Froufe-Pérez, F. Scheffold, R. Sapienza, S. Vignolini, and J. J. Sáenz, Light in correlated disordered media, arXiv:2106.13892.

[2] T. Tanabe, K. Nishiguchi, A. Shinya, E. Kuramochi, H. Inokawa, M. Notomi, K. Yamada, T. Tsuchizawa, T. Watanabe, H. Fukuda *et al.*, Fast all-optical switching using ion-implanted silicon photonic crystal nanocavities, Appl. Phys. Lett. **90**, 031115 (2007).

[3] Y. A. Vlasov, M. O'Boyle, H. F. Hamann, and S. J. McNab, Active control of slow light on a chip with photonic crystal waveguides, Nature (London) **438**, 65 (2005).

[4] N. Soleimani, S. Knabe, G. H. Bauer, T. Markvart, and O. L. Muskens, Role of light scattering in the performance of fluorescent solar collectors, J. Photonics Energy **2**, 021801 (2012).

[5] K. Lee and S. A. Asher, Photonic crystal chemical sensors: pH and ionic strength, J. Am. Chem. Soc. **122**, 9534 (2000).

[6] Q. Yang, S. Zhu, W. Peng, C. Yin, W. Wang, J. Gu, W. Zhang, J. Ma, T. Deng, C. Feng, and D. Zhang, Bioinspired fabrication of hierarchically structured, pH-tunable photonic crystals with unique transition, ACS Nano **7**, 4911 (2013).

[7] J. Kobler, B. V. Lotsch, G. A. Ozin, and T. Bein, Vapor-sensitive Bragg mirrors and optical isotherms from mesoporous nanoparticle suspensions, ACS Nano **3**, 1669 (2009).

[8] O. M. Maragò, P. H. Jones, P. G. Gucciardi, G. Volpe, and A. C. Ferrari, Optical trapping and manipulation of nanostructures, Nat. Nanotechnol. **8**, 807 (2013).

[9] F. Giavazzi, D. Brogioli, V. Trappe, T. Bellini, and R. Cerbino, Scattering information obtained by optical microscopy: Differential dynamic microscopy and beyond, Phys. Rev. E **80**, 031403 (2009).

[10] D. S. Wiersma, Disordered photonics, Nat. Photonics **7**, 188 (2013).

[11] J. D. Forster, H. Noh, S. F. Liew, V. Saranathan, C. F. Schreck, L. Yang, J.-G. Park, R. O. Prum, S. G. J. Mochrie, C. S. O'Hern *et al.*, Biomimetic isotropic nanostructures for structural coloration, Adv. Mater. **22**, 2939 (2010).

[12] P. García, R. Sapienza, Á. Blanco, and C. López, Photonic glass: A novel random material for light, Adv. Mater. **19**, 2597 (2007).

[13] S.-H. Kim, S. Y. Lee, S.-M. Yang, and G.-R. Yi, Self-assembled colloidal structures for photonics, NPG Asia Mater. **3**, 25 (2011).

[14] V. A. Turek, Y. Francescato, P. Cadinu, C. R. Crick, L. Elliott, Y. Chen, V. Urland, A. P. Ivanov, L. Velleman, M. Hong *et al.*, Self-assembled spherical supercluster metamaterials from nanoscale building blocks, ACS Photonics **3**, 35 (2016).

[15] L. Schertel, L. Siedentop, J.-M. Meijer, P. Keim, C. M. Aegerter, G. J. Aubry, and G. Maret, The structural colors of photonic glasses, Adv. Opt. Mater. **7**, 1900442 (2019).

[16] R. Carminati and J. C. Schotland, *Principles of Scattering and Transport of Light* (Cambridge University Press, Cambridge, 2021).

[17] C. W. Hsu, B. Zhen, W. Qiu, O. Shapira, B. G. DeLacy, J. D. Joannopoulos, and M. Soljačić, Transparent displays enabled by resonant nanoparticle scattering, Nat. Commun. **5**, 3152 (2014).

[18] O. Leseur, R. Pierrat, and R. Carminati, High-density hyperuniform materials can be transparent, Optica **3**, 763 (2016).

[19] E. Arbabi, A. Arbabi, S. M. Kamali, Y. Horie, and A. Faraon, Multiwavelength polarization-insensitive lenses based on dielectric metasurfaces with meta-molecules, Optica **3**, 628 (2016).

[20] K. Vynck, R. Pacanowski, A. Dufay, X. Granier, and P. Lalanne, The visual appearances of disordered optical metasurfaces Nat. Mater. (2022), doi: 10.1038/s41563-022-01255-9.

[21] K. Busch, S. Lölkes, R. B. Wehrspohn, and H. Föll, *Photonic Crystals: Advances in Design, Fabrication, and Characterization* (John Wiley & Sons, New York, 2006).

[22] C. F. Bohren and D. R. Huffman, *Absorption and Scattering of Light by Small Particles* (John Wiley & Sons, New York, 1998).

[23] K. Busch and C. M. Soukoulis, Transport Properties of Random Media: A New Effective Medium Theory, Phys. Rev. Lett. **75**, 3442 (1995).

[24] V. Hwang, A. B. Stephenson, S. Magkiriadou, J.-G. Park, and V. N. Manoharan, Effects of multiple scattering on angle-independent structural color in disordered colloidal materials, Phys. Rev. E **101**, 012614 (2020).

[25] S. G. Romanov, T. Maka, C. M. Sotomayor Torres, M. Müller, R. Zentel, D. Cassagne, J. Manzanares-Martinez, and C. Jouanin, Diffraction of light from thin-film polymethylmethacrylate opaline photonic crystals, Phys. Rev. E **63**, 056603 (2001).

[26] R. Ruppin, Validity range of the Maxwell-Garnett theory, Phys. Status Solidi (b) **87**, 619 (1978).

[27] A. Shivola, *Electromagnetic Mixing Formulas and Applications*, IEE electromagnetic waves series (IET, London, 1999) pp. 239–244.

[28] W. T. Doyle, Optical properties of a suspension of metal spheres, Phys. Rev. B **39**, 9852 (1989).

[29] C. A. Grimes and D. M. Grimes, Permeability and permittivity spectra of granular materials, Phys. Rev. B **43**, 10780 (1991).

[30] R. Rezvani Naraghi, S. Sukhov, J. J. Sáenz, and A. Dogariu, Near-Field Effects in Mesoscopic Light Transport, Phys. Rev. Lett. **115**, 203903 (2015).

[31] A. García-Etxarri, R. Gómez-Medina, L. S. Froufe-Pérez, C. López, L. Chantada, F. Scheffold, J. Aizpurua, M. Nieto-Vesperinas, and J. J. Sáenz, Strong magnetic response of submicron silicon particles in the infrared, Opt. Express **19**, 4815 (2011).

[32] A. I. Kuznetsov, A. E. Miroshnichenko, M. L. Brongersma, Y. S. Kivshar, and B. Luk'yanchuk, Optically resonant dielectric nanostructures, Science **354**, aag2472 (2016).

[33] S. Fraden and G. Maret, Multiple Light Scattering from Concentrated, Interacting Suspensions, Phys. Rev. Lett. **65**, 512 (1990).

[34] M. J. Mendes, I. Tobías, A. Martí, and A. Luque, Light concentration in the near-field of dielectric spheroidal particles with mesoscopic sizes, Opt. Express **19**, 16207 (2011).

[35] A. Ashkin and J. M. Dziedzic, Observation of optical resonances of dielectric spheres by light scattering, Appl. Opt. **20**, 1803 (1981).

[36] P. Yazhgur, G. J. Aubry, L. S. Froufe-Pérez, and F. Scheffold, Light scattering from colloidal aggregates on a hierarchy of length scales, Opt. Express **29**, 14367 (2021).

[37] M. Reufer, L. F. Rojas-Ochoa, S. Eiden, J. J. Sáenz, and F. Scheffold, Transport of light in amorphous photonic materials, Appl. Phys. Lett. **91**, 171904 (2007).

[38] G. J. Aubry, L. Schertel, M. Chen, H. Weyer, C. M. Aegerter, S. Polarz, H. Cölfen, and G. Maret, Resonant transport and

near-field effects in photonic glasses, Phys. Rev. A **96**, 043871 (2017).

[39] L. Schertel, I. Wimmer, P. Besirske, C. M. Aegerter, G. Maret, S. Polarz, and G. J. Aubry, Tunable high-index photonic glasses, Phys. Rev. Materials **3**, 015203 (2019).

[40] A. V. Malinka, Analytical expressions for characteristics of light scattering by arbitrarily shaped particles in the WKB approximation, J. Opt. Soc. Am. A **32**, 1344 (2015).

[41] S. K. Sharma and D. J. Sommerford, *Light Scattering by Optically Soft Particles: Theory and Applications* (Springer-Verlag, Berlin Heidelberg, 2006).

[42] H. C. van de Hulst, *Light Scattering by Small Particles* (Dover Publications, New York, 1981).

[43] E. A. Hovenac and J. A. Lock, Assessing the contributions of surface waves and complex rays to far-field Mie scattering by use of the Debye series, J. Opt. Soc. Am. A **9**, 781 (1992).

[44] P. Lindner and T. Zemb (eds.), *Neutron, X-ray and Light Scattering: Introduction to an Investigative Tool for Colloidal and Polymeric Systems, European Workshop on Neutron, X-ray and Light Scattering as an Investigative Tool for Colloidal and Polymeric Systems, Bombannes, France, 1990* (North Holland, Amsterdam, 1991).

[45] D. S. Saxon, *Lectures on the Scattering of Light*, University of California, Los Angeles. Dept. of Meteorology. Scientific report, no. 9 (University of California, Los Angeles, 1955).

[46] K. Shimizu, Modification of the Rayleigh–Debye approximation, J. Opt. Soc. Am. **73**, 504 (1983).

[47] J. E. Gordon, Simple method for approximating Mie scattering, J. Opt. Soc. Am. A **2**, 156 (1985).

[48] J. D. Klett and R. A. Sutherland, Approximate methods for modeling the scattering properties of nonspherical particles: Evaluation of the Wentzel–Kramers–Brillouin method, Appl. Opt. **31**, 373 (1992).

[49] V. Baranau and U. Tallarek, Random-close packing limits for monodisperse and polydisperse hard spheres, Soft Matter **10**, 3826 (2014).

[50] D. W. Mackowski and M. I. Mishchenko, A multiple sphere t-matrix fortran code for use on parallel computer clusters, J. Quant. Spectrosc. Radiat. Transfer **112**, 2182 (2011).

[51] N. Muller, J. Haberko, C. Marichy, and F. Scheffold, Silicon hyperuniform disordered photonic materials with a pronounced gap in the shortwave infrared, Adv. Opt. Mater. **2**, 115 (2014).

[52] K. Edagawa, S. Kanoko, and M. Notomi, Photonic Amorphous Diamond Structure with a 3D Photonic Band Gap, Phys. Rev. Lett. **100**, 013901 (2008).

[53] M. A. Klatt, P. J. Steinhardt, and S. Torquato, Phoamtonic designs yield sizeable 3D photonic band gaps, Proc. Natl. Acad. Sci. USA **116**, 23480 (2019).

[54] J. Ricouvier, P. Tabeling, and P. Yazhgur, Foam as a self-assembling amorphous photonic band gap material, Proc. Natl. Acad. Sci. USA **116**, 9202 (2019).

[55] Neglecting the shape curvature is equivalent to treating the scattering from the global particle assembly, with mean index m_{eff}, in the mRGD approximation.

[56] J.-P. Hansen and I. R. McDonald, *Theory of Simple Liquids* (Academic Press, New York, 1990).

[57] M. A. Odete, F. C. Cheong, A. Winters, J. J. Elliott, L. A. Philips, and D. G. Grier, The role of the medium in the effective-sphere interpretation of holographic particle characterization data, Soft Matter **16**, 891 (2020).

[58] https://doi.org/10.5281/zenodo.6627563.